# Static and high-frequency electric fields in silicon MOS and MS structures probed by optical second-harmonic generation

C. Ohlhoff, G. Lüpke, C. Meyer, and H. Kurz
*Institute of Semiconductor Electronics II, Rheinisch-Westfälische Technische Hochschule, D-52056 Aachen, Germany*
(Received 26 June 1996)

We present a comprehensive analysis of the effects of static and high-frequency electric fields in silicon metal-oxide-semiconductor (MOS) and metal-semiconductor (MS) structures on optical second-harmonic generation (SHG). First, a general Green's function formalism developed by Sipe [J. Opt. Soc. Am. B **4**, 481 (1987)] is applied to determine the voltage dependence of the SHG response from planar MOS structures. This approach takes directly into account the spatial distribution of the dc-electric-field across the silicon space-charge region. Predictions of the theory are in good agreement with experimental results of the SHG bias dependence from MS and MOS structures. Furthermore, the azimuthal SHG anisotropy from Si(111) MOS and Si(001) MS interfaces is determined in the presence of a reverse bias allowing a clear separation of various anisotropic contributions resulting from inhomogeneous bias fields and anisotropic $\chi^{(2)}$ or $\chi^{(3)}$ tensor elements. Finally, we demonstrate the capability of optical SHG for time-resolved measurements of free-running GHz signals on silicon millimeter-wave devices. Consequences for circuit testing are discussed. [S0163-1829(97)01307-6]

## I. INTRODUCTION

Today silicon is the dominant semiconductor for electronic circuits and devices operating at frequencies below 1 GHz. Because of new device technologies silicon has also emerged recently as a viable material for many circuit applications in the millimeter-wave range up to now completely dominated by the III-V technology.[1] Resonator, mixer, and detector circuits realized with Schottky and impact avalanche transit-time diodes, and integrated in planar Si monolithic millimeter-wave integrated circuits (MMIC's) open the way for the development of single-chip transmitters and receivers in the region above 60 GHz. However, these advanced high-speed Si MMIC's demand new measurement techniques with high temporal and spatial resolution.

Optical techniques based on ultrashort laser pulses combine such a high time resolution with the advantages of external probing such as spatial mapping. Earlier optical approaches for measuring voltage wave forms in an integrated circuit (IC) relied on either sensing the induced electric field in an external electro-optic crystal brought near the circuit or bonding the signal out to the electro-optic crystal.[2] Hence these methods introduced unwanted parasitics into the circuit.[3] Later work done in this field relied directly on the birefringence of the GaAs substrate. Using this technique, direct electro-optic sampling of both analog and digital electrical signals in GaAs IC's has been demonstrated.[4,5] Direct electro-optic detection in silicon is not possible because of its centrosymmetric crystal structure. Alternative techniques used for measuring high-speed electrical signals in silicon IC's include the voltage-contrast scanning electron microscope[6] (SEM) and the scanning photoexcitation probe.[7] However, the voltage-contrast SEM has a low sensitivity and the photoexcitation probe, which uses an above-band-gap optical source to perturb photoconductively internal nodes within an integrated circuit, is invasive and only measures the logic states of the circuit. Based on the perturbation of the index of refraction by free carriers, Bloom and coworkers developed a noninvasive optical technique for detecting charge density modulation in silicon integrated devices.[8] Although measurements of real-time 0.8-V digital signals in silicon bipolar junction transistors have been demonstrated, application of this method is limited, because for testing the laser beam must be focused through the backside of the Si substrate. Other higher-order interactions such as optical Kerr and Franz-Keldysh effects are not large enough for the picosecond lasers used in the past to be of practical importance.

However, with the advent of the Kerr-lens-mode-locked Ti:sapphire laser generating sub-100-fs pulses of about 10-nJ pulse energy at a repetition rate of $\sim$80 MHz, nonlinear optical techniques become attractive for contactless sampling of high-frequency electrical signals on silicon millimeter-wave circuits. Several groups have recently demonstrated the capability of optical second-harmonic generation (SHG) for probing static electric fields in crystalline silicon metal-oxide-semiconductor (MOS) and metal-semiconductor (MS) structures,[9–12] and Si/electrolyte and Si/$SiO_2$/electrolyte interfacial regions[13–15] modulated by an external bias. Very recently, we have applied electric field-induced SHG (EFISHG) for monitoring continuous microwave signals on free-running silicon millimeter-wave circuits.[16] Furthermore, Nahata *et al.* conducted time-resolved EFISHG measurements of picosecond electrical pulses propagating on a coplanar waveguide transmission line fabricated on silicon.[17] From these experiments they infer an intrinsic response time of $<10$ fs for EFISHG due to the electronic nature of the SHG process and the short escape length for the reflected second-harmonic (SH) radiation. However, despite this auspicious beginning, these studies have only begun elucidating the complex behavior of potential-induced band bending, the dynamics of photogenerated carriers in the depletion layer, and the spatial distribution of the electric field inside the

 

space-charge region (SCR) in affecting nonlinear optical phenomena.[18] Although a simple phenomenological model for EFISHG from $Si/SiO_2$-electrolyte interfaces has been developed by Aktsipetrov and co-workers,[19,13] deviations from the predicted quadratic SHG bias dependence have already been observed, and attributed to mobile charges and carrier degeneracy.[9,20] In addition, the width of the SCR in silicon which depends on the doping concentration and the applied voltage may be comparable with the SH wavelength and penetration depth. Thus, retardation effects and the interference of field dependent and independent SH contributions can strongly influence the bias dependence of the EFISHG response.[20]

In this work, we present a comprehensive study of the effect of static and high-frequency electric fields on the SH response from silicon MOS and MS structures generated by ultrashort laser pulses. The outline of this paper is as follows. In Sec. II we calculate the voltage dependence of the SH response from silicon MOS structures based on a Green's function formalism developed by Sipe for surface optics.[21] Section III describes the experimental methods and silicon MOS and MS structures used for EFISHG. In Sec. IV we present measurements of the azimuthal SHG anisotropy from Si(111) MOS and Si(001) MS interfaces in the presence of a reverse bias allowing a clear separation of various anisotropic contributions resulting from inhomogeneous bias fields and anisotropic $\chi^{(2)}$ or $\chi^{(3)}$ tensor elements. Furthermore, predictions of the theory developed in Sec. II are compared with experimental results of the SHG voltage dependence from MS and MOS structures. Finally, we demonstrate the capability of EFISHG for time-resolved measurements of free-running GHz signals on silicon millimeter-wave devices. Concluding remarks are given in Sec. V.

## II. GREEN'S FUNCTION FORMALISM FOR EFISHG

So far the relationship between the voltage dependence of the EFISHG response and its source volume has neither been studied experimentally nor theoretically in a systematic way. In the majority of publications concerned with EFISHG in silicon MOS structures the interpretation of the data is based on a simple approximation for the static electric field $\vec{\mathcal{E}}$ in the silicon SCR, introduced by Aktsipetrov and co-workers.[19] In that work, $\vec{\mathcal{E}}$ which varies over the silicon SCR, is approximated by an effective field $\vec{\mathcal{E}}_{\rm eff} \propto (U - U_{\rm fb})$ near the $Si/SiO_2$ interface, and the extension $d_{\rm SCR}$ of the SCR is assumed to be voltage independent resulting in a quadratic dependence of the electric-field-induced SH intensity with surface band bending.[13] However, this approximation is only valid if the SH escape depth $d^{2\omega} \gg d_{\rm SCR}$. Hence Aktsipetrov and coworkers have developed a refined phenomenological model that takes nonlinear interference and retardation effects of the EFISHG response into account.[20] Furthermore, they demonstrated the influence of the spatial distribution of the dc-electric field inside the silicon SCR on EFISHG.

To account for the variation of $\vec{\mathcal{E}}$ across the silicon SCR, it is useful to apply a general Green's function formalism developed by Sipe for surface optics.[21] This approach yields a

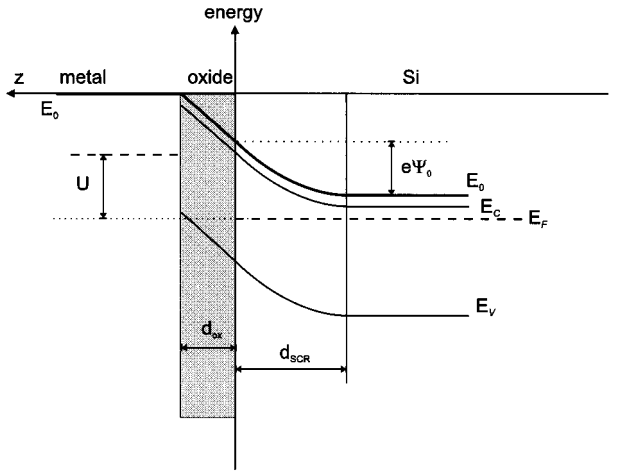


FIG. 1. Energy-band diagram for an ideal $n$-type MOS diode in depletion with $E_0$ the vacuum level, $e\psi_0$ the band bending at the $Si/SiO_2$ interface, $d_{\rm ox}$ the oxide thickness, and $d_{\rm SCR}$ the width of the space-charge region.

solution of Maxwell's equations for a general $n$th-order polarization $\vec{P}^{(n)}$ of the form

$$\vec{P}^{(n)}(\vec{r}) = \int \frac{dK}{(2\pi)^2} \vec{\mathcal{P}}(\vec{K},z) \exp\{i(\vec{K}\cdot\vec{R} - \Omega t)\}, \qquad (1)$$

where $\vec{\mathcal{P}}$ is the Fourier-transform of the polarization at the position $\vec{R}$ in the $x$-$y$ plane parallel to the surface and $\vec{K}$ denotes the wave-vector component at the frequency $\Omega$ parallel to the surface. In the following we consider for the incident input field a transverse monochromatic plane wave of the form

$$\vec{E}^{\omega} = (\vec{E}_p + \vec{E}_s) \exp\{i(\vec{\kappa}\vec{R} - wz - \omega t)\}, \qquad (2)$$

with $\vec{\kappa}$ and $w$ the wave-vector components parallel and normal to the surface. We further assume that the static electric field $\vec{\mathcal{E}}$ consists only of a component in the $z$ direction normal to the surface along which $\vec{\mathcal{E}}$ only varies. This restriction is satisfied for the SCR field produced by a bias voltage applied to a silicon MOS structure as depicted in Fig. 1. In the case of carrier depletion in the $x$-$y$ plane, we obtain

$$\vec{P}^{(3)}(\vec{r}) = \vec{\mathcal{P}}(\kappa,z) \exp\{2i(\vec{\kappa}\vec{R} - \omega t)\}, \qquad (3)$$

with

$$\vec{\mathcal{P}}(\kappa,z) = \chi_D^{(3)} : \vec{\mathcal{E}}(z)(\vec{E}_p + \vec{E}_s)(\vec{E}_p + \vec{E}_s) \exp(-2iwz)$$
$$\equiv \vec{\Gamma} \exp(-2iwz)(z + d_{\rm SCR}), \qquad (4)$$

where $\chi_D^{(3)}$ is the bulk third-order dipole susceptibility tensor, and for $n$-type Si the spacecharge field is given by

$$\vec{\mathcal{E}}(z) = \frac{N_D e}{\epsilon_0 \epsilon_{\rm Si}} (z + d_{\rm SCR}) \hat{z}, \qquad (5)$$

with $-d_{\rm SCR} \leq z \leq 0$ (see Fig. 1), $\epsilon_{\rm Si}$ the static dielectric permittivity of Si, and $N_D$ the donor concentration. The vector $\vec{\Gamma}$ defined in Eq. (4) contains all contributions of $\vec{\mathcal{P}}$ which are

independent of $z$. Next we calculate the field-induced second-harmonic wave $\vec{E}_{fi}^{2\omega}=(\vec{E}_p^{2\omega}+\vec{E}_s^{2\omega})\exp\{i(\vec{K}_0\vec{R}+W_0z-2\omega t)\}$ generated in medium 1 and reflected into medium 0, which is given by

$$\vec{E}_p^{2\omega}+\vec{E}_s^{2\omega}=8\pi i\omega^2c^{-2}W_1^{-1}(\hat{s}T_{01}^s\hat{s}+\hat{p}_0T_{01}^p\hat{p}_1)\vec{\Gamma}\mathcal{L}, \quad (6)$$

where $\mathcal{L}$ denotes the following integral:

$$\mathcal{L}=\int_{-d_{\mathrm{SCR}}}^{0}\exp\{-i(W_1+2w_1)z\}(z+d_{\mathrm{SCR}})dz, \quad (7)$$

with $W_i$ and $\vec{K}_i=2\vec{\kappa}$ the complex SH wave-vector components in medium $i=0,1$ normal and parallel to the surface, and $T_{01}^{s,p}$ the Fresnel transmission tensors. The unit vectors $\hat{s}$, and $\hat{p}_i$ define the directions normal to the plane of incidence and perpendicular to the wave vector $2\vec{\kappa}+W_i\hat{z}$ in the plane of incidence, respectively. Equation (7) can be solved analytically:

$$\mathcal{L}=\frac{1}{(2w_1+W_1)^2}[1-\exp\{id_{\mathrm{SCR}}(2w_1+W_1)\}]+\frac{id_{SCR}}{2w_1+W_1}. \quad (8)$$

Depending on the penetration depth of the fundamental and SH wave, we obtain two different approximations for Eq. (8):

(1) For an effective penetration depth $\alpha_{\mathrm{eff}}^{-1}=\mathrm{Im}(2w_1+W_1)^{-1}\ll d_{\mathrm{SCR}}$, $\mathcal{L}$ can be approximated by

$$\mathcal{L}\approx\frac{id_{\mathrm{SCR}}}{2w_1+W_1}+O(1/[2w_1+W_1]^2)\propto\sqrt{\psi_0}, \quad (9)$$

with $\psi_0\equiv\psi(z=0)$ the Si surface potential (see Fig. 1).

(2) For $\alpha_{\mathrm{eff}}^{-1}\gg d_{\mathrm{SCR}}$ and $\lambda\gg d_{\mathrm{SCR}}$, the exponential function in Eq. (8) can be expanded into a Taylor series yielding

$$\mathcal{L}\approx d_{\mathrm{SCR}}^2+O(d_{\mathrm{SCR}}[2w_1+W_1])\propto\psi_0. \quad (10)$$

Thus, in the first (second) case the SH intensity $I^{(2\omega)}(\psi_0)$ exhibits a linear (quadratic) dependence on the band bending $\psi_0(U)$. To determine $I^{(2\omega)}(U)$, $\psi_0$ must be derived as a function of externally applied voltage $U$:

$$\psi_0=\left\{-\frac{\alpha}{2}+\frac{1}{2}\sqrt{\alpha^2-4(U-U_{\mathrm{fb}})}\right\}^2 \quad (11)$$

$$\overset{\alpha\ll1}{\approx}-(U-U_{\mathrm{fb}})-\alpha\sqrt{U_{\mathrm{fb}}-U}, \quad (12)$$

with $\alpha=d_{\mathrm{ox}}\sqrt{2e\epsilon_{Si}N_D/\epsilon_0\epsilon_{\mathrm{ox}}^2}$, $\epsilon_{\mathrm{ox}}$ the static dielectric permittivity of $SiO_2$, and $d_{\mathrm{ox}}$ the oxide thickness. Since $d_{\mathrm{SCR}}\propto\sqrt{N_D}$, it varies by orders of magnitudes in semiconductors. In the case of depletion, $d_{\mathrm{SCR}}$ varies typically between 25 nm ($N_D=10^{18}\ \mathrm{cm}^{-3}$) and 8 $\mu$m ($N_D=10^{13}\ \mathrm{cm}^{-3}$) in silicon. If $\alpha_{\mathrm{eff}}^{-1}\gg d_{\mathrm{SCR}}\sim\lambda$ (case 2), then $I^{(2\omega)}(U)$ will exhibit bias-dependent oscillations imposed on the quadratic voltage dependence, because of the exponential function in Eq. (8). These modulations in $I^{(2\omega)}(U)$ have indeed been observed experimentally by Aktsipetrov *et al.*[20] The calculations performed here for carrier depletion can be carried out analogously for accumulation, for which a two-dimensional polarization sheet located at the $Si/SiO_2$ interface can be used because of $d_{\mathrm{SCR}}\ll\lambda$. Note, that then the vector $\vec{\Gamma}$ must be defined accordingly.

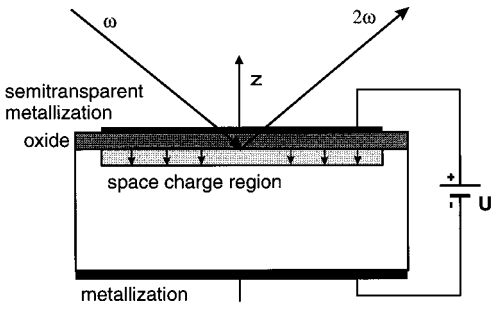


FIG. 2. Experimental geometry for EFISHG from a MOS structure.

## III. SAMPLES AND EXPERIMENTAL METHODS

For EFISHG measurements two laser systems have been used: a regenerative Nd:YLF amplifier, and a modelocked Ti:sapphire laser pumped by the SH radiation from a modelocked Nd:YLF oscillator. The experimental setups for these two laser systems have been described previously in Refs. 16,22. Because of the low energy (4 nJ) of the 100-fs pulses generated by the Ti:sapphire laser at 75.6-MHz repetition rate, the laser beam has been focused on the sample to a 10-$\mu$m spot diameter under a 45° angle of incidence, thereby reaching peak intensities of 1 – 10 GW/cm$^2$ necessary for EFISHG. In contrast, the 2.5-mJ energy of the 40-ps pulses delivered by the Nd:YLF amplifier at 1 kHz repetition rate is high enough to yield unfocused (1.2-mm spot diam.) peak intensities of $\sim 1\,GW/\mathrm{cm}^2$. In all experiments the reflected SH signal is detected by a photon counting system after passing through dispersive elements and color filters suppressing the fundamental radiation by a factor of $\sim 10^{-16}$. The sample is mounted on a rotation and $x$-$y$-translation stage oriented horizontally to the optical table.

All samples have been fabricated on $n$-doped silicon substrates. A thermal oxide underneath a 3-nm Cr and 6-nm Au cap layer is used for the Si(111)-MOS structure. An Ohmic aluminum back metallization allowed us to apply $|U|\leqslant 10$ V bias, yielding a homogeneous electric field $\vec{\mathcal{E}}$ oriented in $z$ direction, as shown in Fig. 2. The advantage of this sample is the simple field geometry for which the EFISHG response is predicted by the one-dimensional model given in Sec. II. Table I summarizes the most important parameters of our MOS and MS structures. For EFISHG measurements on Schottky contacts different microstrip structures, as shown in Fig. 3, have been fabricated on Si(100) substrates of different doping levels by a standard lithography process. By applying a bias to two adjacent microstrip lines forward and reversed biased Schottky contacts are formed at the metal/silicon interfaces as depicted in Fig. 4. The applied voltage almost completely drops over the depletion region of the reversed biased Schottky contact, which is extended from the contact area enabling part of the depletion electric field $\vec{\mathcal{E}}$, which is located within a few 10 nm at the Si surface, to be probed by EFISHG. In contrast to the MOS structure, $\vec{\mathcal{E}}$ is oriented

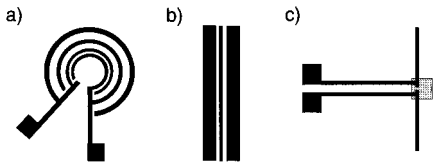


FIG. 3. Schematic of MS structures: (a) ring structure, (b) coplanar transmission line (CTL), and (c) photoconductive antenna on a silicon-on-sapphire substrate. Dimensions are given in the text.

preferentially parallel to the surface of the MS structures. Furthermore, these structures are often used in high-frequency devices, for example, the coplanar transmission line (CTL) shown in Fig. 3(b) is integrated in Si MMIC's to connect different circuit parts. The Cr/Au microstrip electrodes fabricated by a standard liftoff process on a high-Ohmic Si substrate (>2000 Ω cm) to reduce free-carrier-induced damping consist of a 20-$\mu$m-wide signal line separated by 15-$\mu$m-wide gaps from the grounded lines.

For a high-frequency application of the EFISHG technique we utilized a photoconductive dipole antenna [Fig. 3(c)] commonly applied for the detection of coherent free-space submillimeter waves in time-resolved THz-spectroscopy experiments. The antenna structure is fabricated on an ion-implanted silicon-on-sapphire substrate to reduce the carrier lifetime to $<1$ ps. The Hertzian dipole consists of a 50-$\mu$m-long and 10-$\mu$m-wide Au strip with a 5-$\mu$m slot in the center. The two arms are connected to a CTL, which is linked to contact pads of 300 $\mu$m$\times$300 $\mu$m. The ion-implanted Si, which is removed except for a mesa with the Hertzian dipole on top of it, possesses no crystalline order as revealed by Rutherford backscattering experiments, hence only isotropic $\chi^{(2)}$ and $\chi^{(3)}$ tensor elements contribute to the SH response.

## IV. RESULTS AND DISCUSSION

### A. Anisotropic $\chi^{(3)}$ and inhomogeneous electric fields

Within the electric dipole approximation SHG is symmetry forbidden in the bulk of centrosymmetric media, such as

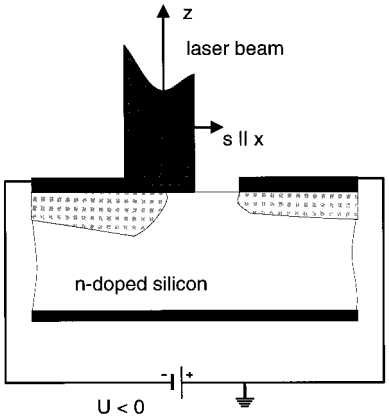


FIG. 4. Schematic of two microstrip lines forming forward and reversed biased Schottky contacts with the underlying $n$-Si substrate. The depletion region of the contact is extended from the contact area enabling the depletion electric field $\mathcal{E}$ to be probed optically. The plane-of-incidence is normal to the projected plane.

TABLE I. Summary of device parameters, where $\rho$ is the specific dark resistance.

| Contact | Geometry | Doping ($cm^{-3}$) | $\rho$ ($\Omega$ cm) | Metal |
|---|---|---|---|---|
| MOS (111) | planar | $N_D$: $5\times10^{13}$ | 90 | Au/Cr |
| | contact | $N_D$: $5\times10^{18}$ | 0.01 | |
| MS (100) | ring | $N_D$: $5\times10^{16}$ | 0.1 | Al |
| | structure | ($n$): $<10^{13}$ | >2000 | |
| MS (100) | CTL | ($n$): $<10^{13}$ | >2000 | Au/Cr |
| MS (SOS) | antenna | Si, Ne: $>10^{19}$ | $\approx\infty$ | Au/Cr |

Si, $SiO_2$, or noncrystalline metallizations. Hence, in these media the reflected SHG response arises from the surface electric dipole and the bulk electric quadrupole contributions, which can be expressed by an effective field-independent second-order nonlinear susceptibility, $\chi^{(2)}_{\rm eff}$ as those contributions cannot be separated in a single experiment.[23] An external electric field applied to a silicon MOS or MS structure, breaks the inversion symmetry of the Si crystal and allows an electric-field-induced bulk dipole contribution, $\chi^{(3)}_{\rm eff}\mathcal{E}$. Thus, the total EFISHG response

$$I^{2\omega}_{\rm tot}(U)\propto|\chi^{(2)}_{\rm eff}+\chi^{(3)}_{\rm eff}\mathcal{E}|^2, \tag{13}$$

arises from a coherent superposition of field-dependent $\chi^{(3)}_{\rm eff}\mathcal{E}$, and field-independent $\chi^{(2)}_{\rm eff}$ contributions, both containing isotropic and anisotropic components. Furthermore, the rotational anisotropy of the EFISHG signal can be caused by both: anisotropic $\chi^{(2)}$ or $\chi^{(3)}$ components, and inhomogeneous fields $\mathcal{E}(\phi)$, where $\phi$ denotes the rotation angle with respect to the surface normal ($z$ direction) of the sample. To prove the existence of the former one, EFISHG rotational anisotropy measurements have been performed on a planar Si(111)-MOS structure. The space-charge field, $\vec{\mathcal{E}}=\mathcal{E}_z\hat{z}$, in this structure is entirely symmetric with respect to rotations about the surface normal, and therefore any rotational anisotropy of the EFISHG response must arise from anisotropic nonlinear susceptibility components. In this case $I^{2\omega}_{p,p}(U,\phi)$ is given by

$$I^{2\omega}_{p,p}(U,\phi)\propto|a_0(U)+a_3(U)e^{i\psi_3}\cos(3\phi)|^2, \tag{14}$$

where $a_0(U)$ and $a_3(U)$ are the isotropic and threefold contribution, both containing field-independent $\chi^{(2)}$ components and field-dependent contributions of the form $\chi^{(3)}\mathcal{E}_z(U)$. A typical threefold modulation of $I^{2\omega}_{p,p}(U=0\text{V},\phi)$ from the Si(111)-MOS structure measured at a 730-nm fundamental wavelength is presented in Fig. 5(a). In terms of $\Delta^{2\omega}_{p,p}(U,\phi)=I^{2\omega}_{p,p}(U,\phi)-I^{2\omega}_{p,p}(U=0\text{V},\phi)$ the variation of the EFISHG rotational anisotropy with applied bias is demonstrated in Figs. 5(b) and 5(c) for $U=-3.2$ V and $U=+3.0$ V. Note, that the threefold modulation of $\Delta^{2\omega}_{p,p}(U,\phi)$ arises not necessarily from an anisotropic $\chi^{(3)}$ component. Even in the case, when $\chi^{(3)}$ is isotropic and hence $a_3(U)$ bias independent, $\Delta^{2\omega}_{p,p}(U,\phi)$ can be anisotropic due to the interference term, $2\text{Re}(a_0a_3e^{i\psi_3})\cos(3\phi)$. Using the values of $a_i(U=0\text{V})$ deduced from curve (a) the voltage-induced changes, $\delta a_i=|a_i(U)-a_i(U=0V)|$ can be

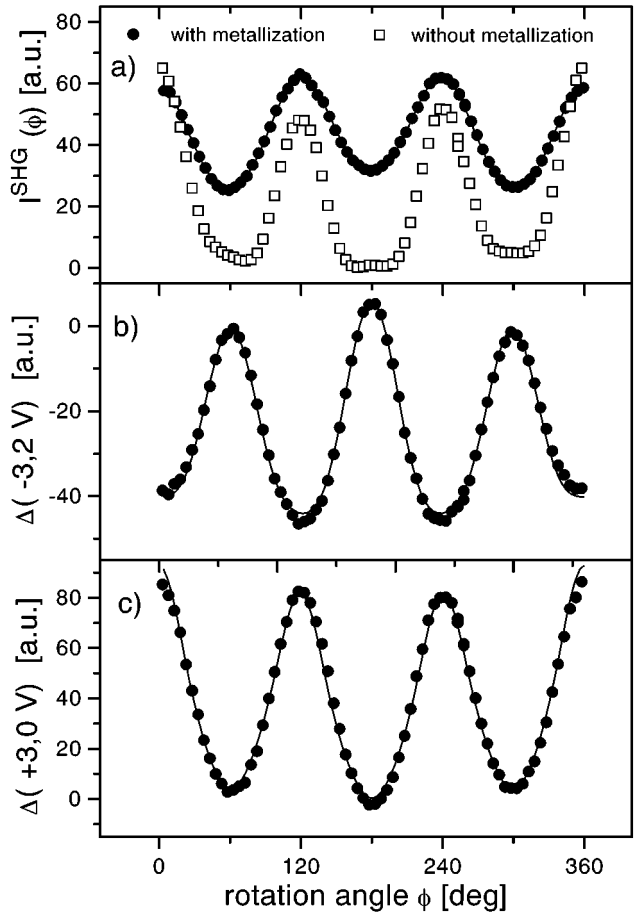


FIG. 5. $p$-in/$p$-out SH rotational anisotropy from the Si(111)-MOS structure at several biases: (a) $I^{(2\omega)}(\phi,U)$ for $U=0$ V, (b) $\Delta=-3.2$ V, and (c) $\Delta=+3.0$ V. Solid curves represent fits of Eq. (14) to data. The fit parameters are listed in Table II.

derived from $\Delta^{2\omega}_{p,p}(U,\phi)$ summarized in Table II for curves (b) and (c). The results show, that $a_0$ and $a_3$ are clearly voltage dependent due to field-dependent isotropic and anisotropic contributions of the form $\chi^{(3)}\mathcal{E}_z(U)$.

The occurrence of a crystal-induced anisotropic EFISHG response depends on the orientation of the substrate. In contrast to the dc-biased (111)-oriented silicon substrate a homogeneous electric field $\vec{\mathcal{E}}=\mathcal{E}_z\hat{z}$ oriented normal to the Si(100) surface will only influence the isotropic parameter $a_0$.[11] However, due to the complex structure of submillimeter wave devices and integrated circuits new interfaces arise, which are not oriented parallel to the $\hat{z}$ axis. The broken inversion symmetry at the interface can give rise to a strong dipole-allowed anisotropic SH response as demonstrated in Fig. 6 for a CTL on a Si(100) substrate. Figure 6(a) displays a line scan of $I^{2\omega}_{s,s}$ normal to the direction of the microstrip lines and the plane of incidence. For the $s$-in/$s$-out polarization combination only a weak SH signal is generated by the anisotropic electric-quadrupole component ($\zeta$) in the Si(100) substrate. However, a strong enhancement of $I^{2\omega}_{s,s}$ at the edges of the transmission lines is clearly visible in Fig. 6. The spatial width of the SHG peak is determined by the focus diameter and not by interfacial properties.

TABLE II. Fourier coefficients in Eq. (14) deduced from the EFISHG data shown in Fig. 5.

| Curve | $a_0$ | $a_3$ | $a_3/a_0$ |
|---|---|---|---|
| (a) | 64, 7 | 15, 3 | 0, 24 |
| | $\delta a_0$ | $\delta a_3$ | $\delta a_3/\delta a_0$ |
| (b) | 36, 8 | 27, 1 | 0, 74 |
| (c) | 43, 1 | 32, 5 | 0, 75 |

Applying a dc-bias to the left ($L$) microstrip line, as indicated in Fig. 6, yields to free-carrier depletion at the reverse biased Schottky-contact, which depending on the polarity of the applied voltage can be the L ($U<0$ V) or $R$ ($U>0$ V) microstrip line. The voltage almost completely drops over the SCR, which is extended further away from the edge of the microstrip line enabling the space-charge field $\vec{\mathcal{E}}\approx\mathcal{E}_x\hat{x}$ to be detected by optical SHG as shown schematically in Fig. 4. Analogously to linear reflectance, the relative index $\beta^{(2\omega)}$ is introduced by $\beta^{(2\omega)}(U)=I^{(2\omega)}(U)/I^{(2\omega)}(U=0\ \text{V})$. In terms of $\beta^{(2\omega)}(U)$ the electric-field dependence of $I^{(2\omega)}_{s,s}$ is monitored in Fig. 6, curves (b) and (c) for $U=-5$ V and $U=+5$ V. The data reveal that the electric-field-induced contribution, which is located at the reverse biased contact, exceeds the voltage independent surface and higher-order contributions to $I^{(2\omega)}_{s,s}$. Furthermore, in contrast to the maxima of the SHG response, which are located at the edges of the transmission lines as shown in Fig 6(a), the positions of the EFISHG maxima are clearly separated from the edges indicating that the SCR is extended parallel to the surface further away from the interface of the Si/Au contact.

To monitor the anisotropy of $I^{(2\omega)}_{s,s}(\phi,U)$ caused by preferential orientation of the static electric field $\vec{\mathcal{E}}\approx\mathcal{E}_x\hat{x}$ a ring structure as shown in Fig. 3(a) can be used. Figure 7 shows $I^{(2\omega)}_{s,s}(\phi,U)$ for two applied voltages, $U=0$ V and 0.65 V, measured at different angles $\phi$ between the $s$-polarized optical fields $\vec{E}^{\omega}$, $\vec{E}^{2\omega}$ and the static electric field $\vec{\mathcal{E}}$, which is oriented normal to the edge of the Al contact. The anisotropic quadrupole SH contribution ($\zeta$) is negligible small for the values of $\phi$ selected, hence no crystal-induced anisotropic contribution to $I^{(2\omega)}_{s,s}(\phi,U)$ is present. Due to the high doping level $N_D=5\times10^{16}\ \text{cm}^{-3}$ of the Si substrate a significant change of the SH response caused by $\mathcal{E}(U)\propto\sqrt{N_D}$ can be observed at voltages $U<1$ V. The rotational anisotropy of $I^{(2\omega)}_{s,s}(\phi,U)$ can be described phenomenologically by

$$I^{(2\omega)}_{s,s}(\phi,U)\sim|a_1(U)\cos(\phi)|^2. \tag{15}$$

The onefold symmetric contribution $a_1(U)$ arises from both, a field-independent $\chi^{(2)}_{xxx}$ component induced by the perturbation of the inversion symmetry normal to the edge of the Al contact, and an electric-field-induced $\chi^{(3)}\mathcal{E}_x(U)\hat{x}$ contribution, both exhibiting $C_{1v}$ symmetry with respect to the Al step edge as shown in the inset of Fig. 7.

### B. Voltage dependence of the SH response

In order to use EFISHG for determining voltage levels in electrical devices and high-frequency circuits, it is necessary to investigate the relationship between the SH response

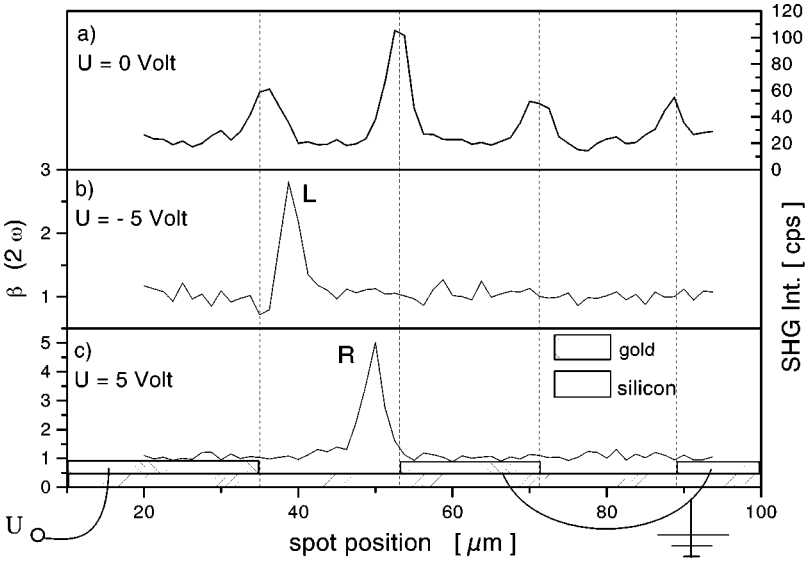


FIG. 6. Line scans of $I_{s,s}^{(2\omega)}$ and $\beta^{(2\omega)}$ from the Au microstrip lines on the Si(100) substrate for different applied voltages $U$: (a) $I_{s,s}^{(2\omega)}$ for $U=0$ V, (b) $\beta^{(2\omega)}$ for $U=-5$ V, and (c) $\beta^{(2\omega)}$ for $U=5$ V.

caused by an electric field $\mathcal{E}(U)$ and the externally applied voltage $U$. As discussed in Sec. II two cases must be distinguished:

(1) If only part of $U$ drops over the probed volume, then an approximately linear dependence is obtained:

$$I^{2\omega}(U)\propto(U-U_{\min}). \tag{16}$$

(2) If $U$ drops completely over the volume generating the EFISHG response, then a quadratic relationship is given:

$$I^{2\omega}(U)\propto(U-U_{\min})^2. \tag{17}$$

Figure 8 shows the voltage dependence of the SH response from a Si(111)-MOS structure. The Si substrate was oriented such that for the ($s$-in, $s$-out) polarization combination the anisotropic SH signal is maximized. For both wavelengths of the fundamental, 730 and 1053 nm, a quadratic voltage dependence of the SH intensity is obtained. While at 730 nm the SH minimum occurs approximately at the flat-band voltage $U_{\rm FB}=-6.7$ V, at 1053 nm it is shifted further

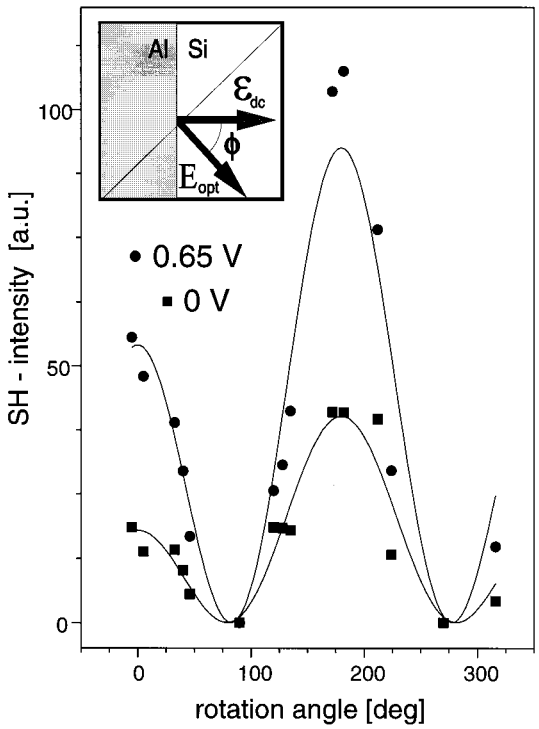


FIG. 7. $I_{s,s}^{(2\omega)}(\phi,U)$ from the Si(100)-MS ring structure for two applied voltages: ■ $U=0$ V, and ● $U=0.65$ V. Solid curves represent fits to data using Eq. (15) plus an isotropic background signal. Inset: Schematic of the optical- and electrical-field configuration at the edge of the Al microstrip line.

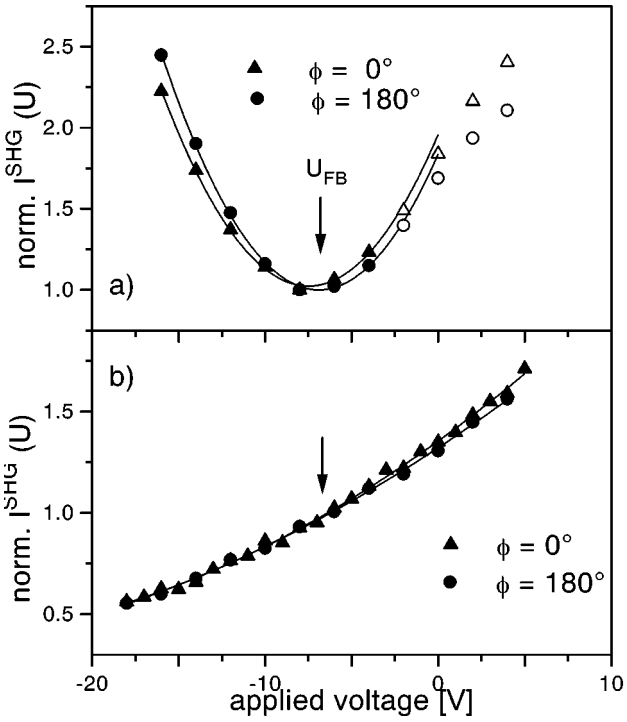


FIG. 8. Voltage dependence of $I_{s,s}^{(2\omega)}$ from a Si(111) MOS structure for two azimuthal orientations, $\phi=0°$ and 180°, and two wavelengths: (a) $\lambda=730$ nm and (b) $\lambda=1053$ nm. Solid curves represent fits of Eq. (1) to the data.

TABLE III. Amplitudes and phases in Eq. 18 deduced from the EFISHG data shown in Fig. 8, and averaged over both angles $\phi=0°$ and 180°.

| Wavelength | $A$ | $B$ | $B/A$ | $\psi_{el}$ |
|---|---|---|---|---|
| (nm) | (–) | ($V^{-1}$) | (V) | |
| 730 | 1, 0 | 0, 13 | 0, 13 | −84° |
| 1053 | 0, 99 | 0, 058 | 0, 059 | 34° |

to more negative potentials due to an interference between the EFISHG response and the field-independent SH contribution as given by

$$I^{2\omega}(U)=|A+B(U-U_{\mathrm{FB}})e^{i\psi_{\mathrm{el}}}|^2. \tag{18}$$

The fit parameters deduced from the curves shown in Fig. 8 are listed in Table III. The data points represented by the open symbols have not been used in the fit as the SH response begins to saturate at these voltages. At 730 nm the phase difference $\psi_{el}$ between the two SH contributions is approximately 90° and hence the minimum of the SH response occurs at $U_{\mathrm{FB}}$. In contrast, at 1053 nm the voltage dependence of the SH signal in the range $-18\ \mathrm{V}<U<6\ \mathrm{V}$ is dominated by the mixed term in Eq. (18):

$$2AB(U-U_{\mathrm{FB}})\cos(34°)>B^2(U-U_{\mathrm{FB}})^2, \tag{19}$$

yielding a minimum of $I^{2\omega}(U)$ at −36 V shifted from the flatband by $\sim -29$ V. In the limit of $A\cos(\psi_{\mathrm{el}})\gg B$, an almost linear $I^{2\omega}-V$ characteristic is obtained, which is of great practical importance for testing high-frequency circuits as shown in a recent work.[16]

Furthermore, at 1053-nm wavelength the absorption length of the SH radiation in Si, $\alpha^{-1}(527\ \mathrm{nm})\sim 1\,\mu\mathrm{m}$, is comparable to the $\sim 2\,\mu$m width of the depletion region for $U<U_{\mathrm{FB}}$ and a doping level $N_D=5\times10^{13}\ \mathrm{cm}^{-3}$ of the Si substrate. For $U>U_{\mathrm{FB}}$ free electrons accumulate at the Si/$SiO_2$ interface and the induced static electric field decreases exponentially over a few nanometers. Hence in both cases, depletion and accumulation of minority carriers, the voltage drops completely over the surface region generating the EFISHG response, which yields to the quadratic $I^{2\omega}-V$ characteristic theoretically predicted. The same characteristic has been found by Aktsipetrov *et al.* in EFISHG experiments conducted on a Si/$SiO_2$/electrolyte interface at a fundamental wavelength of 1064 nm, confirming that in our experiments the field-induced SH contributions from the metallization are negligible.[9]

At a fundamental wavelength of 730 nm, however, a *linear* voltage dependence of the EFISHG signal should be obtained for $U<U_{\mathrm{FB}}$ (carrier depletion), because the absorption length of the harmonic radiation, $\alpha^{-1}(365\ \mathrm{nm})\sim 10\ \mathrm{nm}\ll 2\,\mu$m, is two orders of magnitude smaller and therefore only the electric field near the Si surface contributes to $I^{2\omega}(U)$. However, a quadratic bias dependence of $I^{2\omega}(U)$ has been observed, as displayed in Fig. 8(a). This can be explained by photoexcited carriers screening the electric field, because the photon energy of the fundamental (1.7 eV) exceeds the indirect band-gap energy of Si ($E_{\mathrm{ind}}=1.12$ eV at 300 K), which for an average power of 30 mW, and a focus spot of 10-$\mu$m-diam. yields a density of photogenerated carriers per pulse of $\sim 5\times10^{16}\,\mathrm{cm}^{-3}\gg N_D$. The excited electron-hole pairs will be separated immediately by the depletion electric field, which breaks down within a few picoseconds and remains screened in the time between two subsequent laser pulses (~13 ns), because the lifetime of the minority carriers at the $Si/SiO_2$ interface is typically several 10 ns. The induced surface photovoltage changes the band bending of the illuminated MOS contact, so that the EFISHG response is caused by an electric field extended only a few nm into the Si substrate yielding to a quadratic $I^{2\omega}V$ characteristic as shown in Fig. 8(a). The saturation of curve (a) for $U>0$ V also reveals the influence of photogenerated carriers.

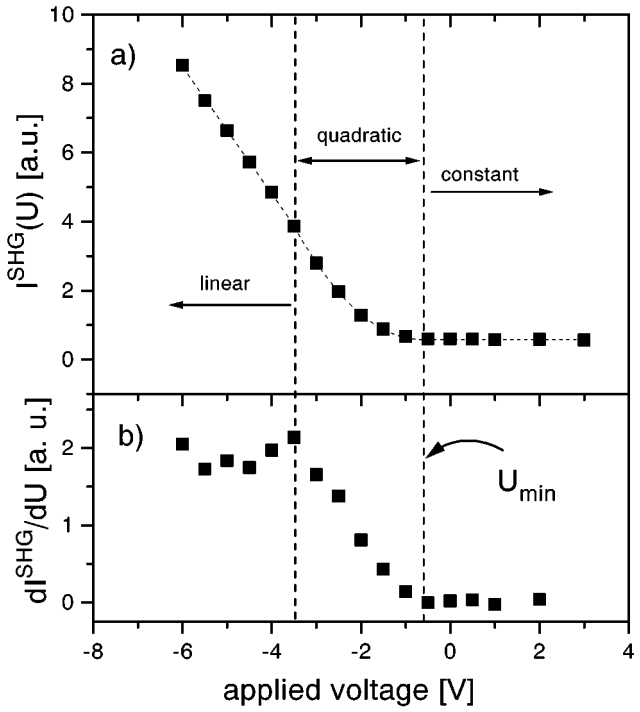


FIG. 9. (a) $I^{(2\omega)}_{s,s}(U)$ and (b) $\partial I^{(2\omega)}_{s,s}(U)/\partial U$ from the left ($L$) MS contact of the microstrip line shown in Fig. 6.

For comparison, the voltage dependence of the SH signal has been measured from the ring structure and the CTL [see Figs. 3(a) and 3(b)]. These structures differ from the MOS contact by two main aspects: First, the electrical characteristic corresponds to that of a metal-semiconductor-metal (MSM) structure, which without an insulator at the interfaces possesses a much lower resistance. An externally applied voltage $U$ drops over the two Schottky contacts connected in series and the high-Ohmic Si substrate in between, because of the nonvanishing current. The second difference is concerned with the field geometry. In contrast to the MOS structure, in which the electric field $\mathcal{E}\equiv\mathcal{E}_z\hat{z}$ is oriented normal to the surface, the EFISHG signal from the MS structures is generated by the electric-field component, $\mathcal{E}_x$, parallel to the surface. Therefore the exact position and diameter $f$ of the focus spot at the edges of the microstrip lines determine the voltage drop over the volume generating the SH signal and hence the bias dependence of the EFISHG response as shown in Fig. 9(a). In this experiment the fundamental and the reflected SH radiation are polarized normal to the plane

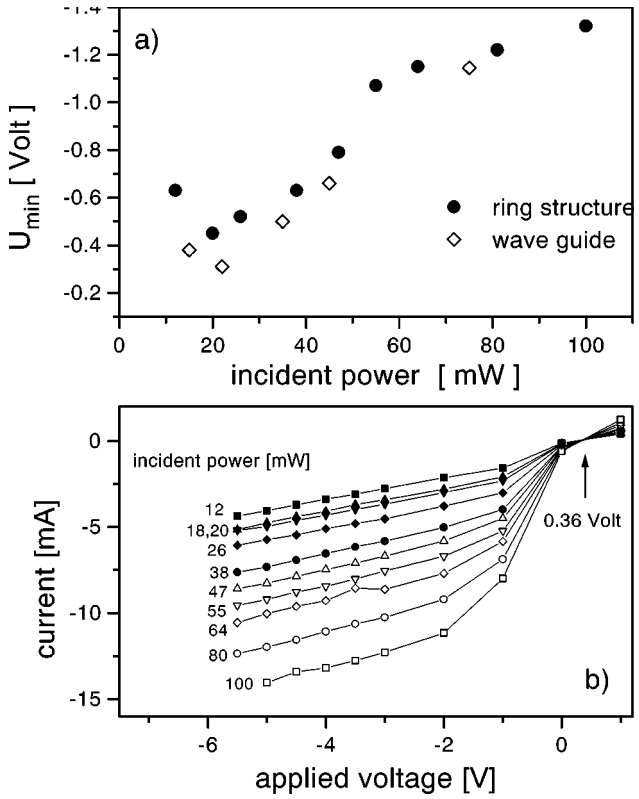


FIG. 10. (a) $U_{\min}$ as a function of incident cw power from the MS ring structure (Al) (full symbols) and the microstrip line (Au/Cr) (hollow symbols), both on a high-Ohmic Si(100) substrate. (b) Dependence of the $I$-$V$ characteristic on the incident cw power.

of incidence and the edge of the metal contact. In Fig. 9(a) three regions can be distinguished in the EFISHG voltage dependence:

(1) For $U>U_{\min}$, the right MS contact ($R$) is driven into depletion, so that its resistance is strongly increased (see Fig. 6). Only a small and approximately constant part of $U$ drops over the left MS contact ($L$) investigated, and therefore the SH signal exhibits no bias dependence.

(2) For $U_{\min}>U>-3.5$ V, the applied voltage drops mainly over the left MS contact, and the EFISHG intensity depends quadratically on $U$, i.e., $f>d$ with $d$ the extension of the SCR along the $x$ axis as depicted in Fig. 4.

(3) For $-3.5$ V$>U$, the SCR exceeds the laser spot diameter, i.e., $d>f$ and $I^{2\omega}(U)$ varies linearly with $U$.

The derivative of $I^{2\omega}(U)$ is shown in Fig. 9(b) to emphasize the three different regions. Clearly visible is the transition from a linear to quadratic $I^{2\omega}$-$V$ characteristic. Note that the voltage dependence of the SH signal begins at $U_{\min}=-0.7$ V and not at the flatband voltage $U_{\rm fb}=0.36$ V, which is not caused by an interference effect, because the field-independent SH response is very small, as shown in Fig. 9. Figure 10(a) reveals that $|U_{\min}|$ strongly increases with incident cw laser power, because the photocurrent $I_{\rm ph}$ and hence the voltage drop over the high-Ohmic Si substrate strongly increase with applied voltage $U$ and cw laser power, as demonstrated in Fig. 10(b). Hence in the region $U_{\rm fb}>U>U_{\min}$ the voltage drop over the Si substrate dominates. Only when $I_{\rm ph}$ reaches saturation at $\sim U_{\min}$ the voltage drop at the MS contact becomes proportional to $(U-U_{\min})$ and $I^{2\omega}(U)$ exhibits the expected voltage dependence. These results demonstrate, that in experiments performed with the Ti:sapphire laser photogenerated free carriers strongly influence the EFISHG response. To reduce the invasiveness of the EFISHG method measurements should be performed at a photon energy of the fundamental below the indirect Si band gap.

Moreover, photoexcited carriers trapped at interfacial defect or impurity centers will also modify the semiconductor surface band bending, thereby altering the second-order nonlinear optical response of the system.[18,24–26] Recently, we have shown that plasma-deposited oxides exhibit a large field-induced SH transient, which is caused by electron trapping at near interface oxide defects.[26] This charge trap induced SH response could be considerably reduced after rapid thermal annealing of the plasma oxide in an inert atmosphere, and was not found for oxides thermally grown at 850 °C as used for our MOS structures. In contrast, the Si substrate of the MS structures was partially covered with a native oxide, for which we indeed observed an oxide charge trap-induced SH transient. However this effect could only be observed using $p$-polarized SH light as the space-charge field associated with trap centers is oriented mainly normal to the $Si/SiO_2$ interface. Hence $s$-polarized EFISHG measurements provide an almost background-free probe of internal electric fields in silicon IC's.

### C. High-frequency EFISHG measurements

Time-resolved optical testing of high-speed electronics can be performed in two ways: for impulsive characterization, a portion of the laser output is used for generating ultra short electrical pulses on the device under test, and the other portion is introduced with a variable temporal delay at a nearby point to sample the electrical pulses.[17] Since pump- and probe-pulses originate from the same laser source, synchronization is not necessary. In contrast, for synchronous optical sampling of high-repetitive voltage wave forms it is necessary to synchronize the fundamental or a higher harmonic of the laser pulse repetition frequency, $f_l$, to the frequency, $f_s$, of the electrical signal.[5] Assuming Dirac-like pulses and an ideal harmonic mixer with unlimited bandwith, an exact replica of the voltage wave form is obtained at an intermediate frequency,

$$f_i=nf_l-f_s. \tag{20}$$

In our experiments, a trigger signal at $f_i\sim 500$ Hz ($n=27$) is used for gating a multichannel data processing unit which sequentially samples the EFISHG signal. The experimental setup is described in Ref. 16. A sinusoidal signal at a frequency $>1$ GHz generated by a microwave synthesizer (Rhode and Schwarz SMP03) is transmitted to a photoconductive antenna [see Fig. 3(c)] via a SMA coaxial cable and non-impedance-adjusted wire bonds. An additional dc bias can be applied to the antenna via an interconnected $T$ base. To achieve a time resolution better than 10 ps the timing jitter has to be limited.[27] We have accomplished this by phaselocking the Ti:sapphire laser to a master oscillator crystal at a frequency $f_l$ of 76.5 MHz by using a commercial timing stabilizer (Lightwave S1000) which controls $f_l$ via the cavity

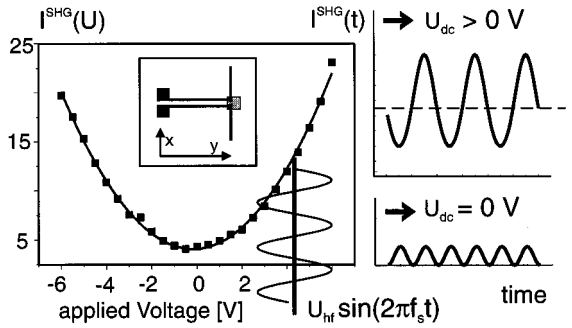


FIG. 11. Dependence of $I_{x,x}^{(2\omega)}$ on the applied dc voltage bias in the slot of a photoconductive antenna. The solid curve represents the parabolic relationship. The inset displays the antenna configuration. The right side shows a schematic of the superposition of a dc bias $U_{\mathrm{dc}}$ and a hf-signal $U_{\mathrm{hf}}\sin(2\pi f_s t)$.

length.[28] This is achieved by moving the output coupler with a piezoelectric transducer. Furthermore, the microwave signal is transmitted to a photoconductive switch, which gated by the laser pulses provides the trigger signal ($f_i$) for the detector. Hence the EFISHG signal from the antenna and the trigger of the detector are phase and frequency synchronized. Absolute time scaling of the microwave signal is achieved by varying the time delay of the laser pulses in the reference arm thereby changing the phase difference between $I^{(2\omega)}(f_i t)$ and the trigger signal.

To calibrate the EFISHG signal from the photoconductive antenna, the $I^{(2\omega)}$-$V$ characteristic has been determined for an applied dc bias. For the ($s$-in, $s$-out) polarization combination, with $\hat{s}$ being parallel to the $x$ direction of the Hertzian dipole arms (see Fig. 11), $I_{s,s}^{(2\omega)}$ is given by

$$I_{s,s}^{(2\omega)} \propto |\chi_{xxx}^{(2)} + \chi_{xxxx}^{(3)} \mathcal{E}_x|^2 I_s^{(\omega)^2} \tag{21}$$

containing two nonlinear susceptibility tensor elements, $\chi_{xxx}^{(2)}$ and $\chi_{xxxx}^{(3)}$. To obtain the voltage dependence of the EFISHG signal, the source term must be integrated over the generating volume. Since the escape depth $d_{\mathrm{ED}}$ of the EFISHG signal is less than 50 nm in our experiments absorption of the fundamental radiation is negligible and walk off is of no importance. Further we assume the fundamental field to be approximately constant across the 5-$\mu$m-wide slot of the photoconductive antenna, since the slot is smaller than the 10-$\mu$m spot diameter. The voltage induced contribution $E^{(2\omega)}(U)$ to the harmonic signal is therefore given by:[29]

$$E_x^{(2\omega)}(U) \propto \int_{\mathrm{slot}} dx \int_{\mathrm{ED}} dz\, \chi_{xxxx}^{(3)} E_x^{(\omega)} E_x^{(\omega)} \mathcal{E}_x$$

$$\propto d_{\mathrm{ED}} \chi_{xxxx}^{(3)} \int_{\mathrm{slot}} dx\, \mathcal{E}_x \propto (U - U_{\mathrm{FB}}), \tag{22}$$

where $U_{\mathrm{FB}}$ is the flatband potential and $U$ denotes the applied voltage. The data shown in Fig. 21 confirms the quadratic $I^{(2\omega)}$-$V$ characteristic expected from Eq. (22). The solid curve is a fit of

$$I^{(2\omega)}(U) = A[1 + \eta(U - U_{\mathrm{min}})^2] \tag{23}$$

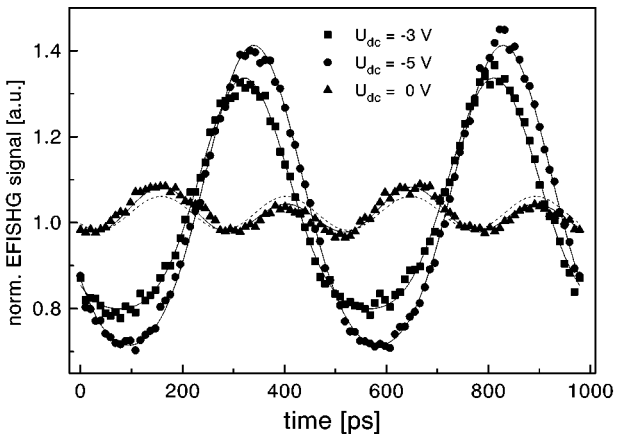


FIG. 12. A freely running 2.043-GHz signal on a photoconductive antenna for different applied bias $U_{\mathrm{dc}}$ sampled with a time resolution of 10 ps. The solid lines represent fits of Eq. (24) with frequency $f_s$, whereas the dashed one is a guide to the eye using a $\sin(4\pi f_s t)$ wave form.

to the data with $\eta = 11.5\times10^{-2}$ V$^{-2}$ and $U_{\mathrm{min}} = -170$ mV. As for the MOS contacts the shift of $U_{\mathrm{min}}$ from the flatband ($\sim -10$ mV) is caused by an interference effect with field-independent $\chi^{(2)}$ contributions, which originate from symmetry perturbation at the silicon/metal interfaces (see Sec. IV B). This additional SH signal causes also the offset of the intensity minimum in Fig. 11.

For time-resolved EFISHG measurements a sinusoidal signal at $f_s = 2.043$ GHz is transmitted to the photoconductive antenna. Since the EFISHG signal is recorded via single photon counting, a lock-in amplifier or gated-integrator cannot be used. Therefore a multichannel data acquisition unit is employed for registering the photomultiplier signal in different channels $s_m$ ($m$ = number of channels in the data acquisition unit) according to the moment the signal is recorded in the time interval $f_i^{-1}$. Since the recording frequency of the data processing unit is limited to $\sim$70 kHz, a low intermediate frequency $f_i \sim 500$ Hz must be used to achieve a resolution better than 10 ps (or $m = 100$ channels). For this method relative time scaling is achieved by using the period of the reference signal, which corresponds to the period $f_s^{-1}$ of the hf signal. According to Eq. 20 the detected $I^{(2\omega)}(s_m)$ histogram yields a replica of the microwave signal $U_{\mathrm{hf}}\sin(2\pi f_s t)$ modified by the nonlinear $I^{(2\omega)}$-$V$ characteristic shown in Fig. 11.

The EFISHG data presented in Fig. 12 show the microwave signal with a time resolution of approximately 10 ps for three different applied bias $U_{\mathrm{dc}}$: $-5$ V (●), $-3$ V (■), and 0 V (▲). The data clearly reveal the combined effect of the applied bias and the microwave signal, $U_{\mathrm{hf}}\sin(2\pi f_s t)$. As shown schematically in Fig. 11, the quadratic $I^{(2\omega)}$-$V$ characteristic causes mixing and superposition of different field-induced SH contributions:

$$I^{(2\omega)}(U) \propto \{1 + \eta[U_{\mathrm{hf}}\sin(2\pi f_s t) + U_{\mathrm{dc}} - U_{\mathrm{min}}]^2\}, \tag{24}$$

Without any bias ($U_{\mathrm{dc}} = 0$ V), (▲), the EFISHG signal exhibits a small modulation $\propto U_{\mathrm{hf}}^2 \sin(4\pi f_s t)$ at twice the frequency of the microwave signal due to the quadratic $I^{(2\omega)}$-$V$ characteristic shown in Fig. 11. Since the EFISHG re-

sponse varies quadratically with $U_{\mathrm{hf}}^2$, the hf field polarity cannot be determined. The observed deviation from a perfect $\sin(4\pi f_s t)$ wave form (dashed curve) can be attributed to an additional contribution $\propto 2U_{\mathrm{hf}}U_{\mathrm{min}}\sin(2\pi f_s t)$ due to the voltage offset $U_{\mathrm{min}}$. Applying a bias of $-3$ V (■) yields a slightly distorted replica of the microwave signal generated by the dominant EFISHG contribution $\propto 2U_{\mathrm{dc}}U_{\mathrm{hf}}\sin(2\pi f_s t)$. The deviation from a pure sinusoidal wave (solid curve) is now caused by the term $\propto U_{\mathrm{hf}}^2\sin(2\pi f_s t)^2$ indicating that $U_{\mathrm{dc}} > U_{\mathrm{hf}}$. Finally, for a bias which is much larger than the hf signal, e.g., $-5$ V (●), the enhanced modulation of the EFISHG response becomes almost linear with respect to the probed microwave signal, $U_{hf}\sin(2\pi f_s t)$. The solid and dashed curves in Fig. 12 are the best fits of Eq. (24) to the experimental data, when we use $\eta = 11.5\times 10^{-2}$ V$^{-2}$ and $U_{\mathrm{min}} = -170$ mV as determined from the static $I^{(2\omega)}$-$V$ characteristic. We are able to deduce a value of $1.0\pm 0.2$ V for the amplitude $U_{\mathrm{hf}}$ of the microwave signal. The good agreement between the fit curves and the experimental data demonstrates that the static $I^{(2\omega)}$-$V$ characteristic is also valid for high-frequency fields. However time-resolved measurements via a multichannel data acquisition unit requires relative long data processing times. If only the amplitude $U_{\mathrm{hf}}$ is of interest and not the entire time wave form, then the recording time can be drastically reduced by frequency domain sampling. For these measurements, the single photon events are counted only by two channels, which are gated alternately with half the period $(1/2f_i^{-1})$ of the reference signal. Analogous to a lock-in amplifier, the difference between the counting rates $\Delta(U_{\mathrm{hf}}) = I^{(2\omega)}(U_{\mathrm{hf}}\sin(2\pi f_i t)) - I^{(2\omega)}(U_{\mathrm{hf}}\sin(2\pi f_i t + \pi))$ is proportional to the average value of the intensity modulation and is independent of time-constant SH contributions, which causes the offset of the high-frequency EFISHG curves in Fig. 12. Since the time wave form of the hf signal is comprised in $\Delta(U_{\mathrm{hf}})$, the data acquisition time is reduced by a factor of $m/2$. Figure 13 shows the EFISHG data obtained via frequency domain sampling of 2- and 10-GHz signals transmitted to the photoconductive antenna. The time scale represents the phase difference between the reference and the EFISHG signal, adjusted with the mechanical delay stage in the reference arm (see Ref. 16). In Fig. 13, the sinusoidal wave form of the data indicated by the solid curves results from the data acquisition, which like a lock in amplifier is only sensitive to the frequency $f_s$ and its odd-numbered higher harmonics. Therefore, detection of the hf signal with this method is only possible when a dc bias is applied, because for $U_{\mathrm{dc}} = 0$ V the EFISHG signal modulates at twice the signal frequency, as shown in Fig. 12.

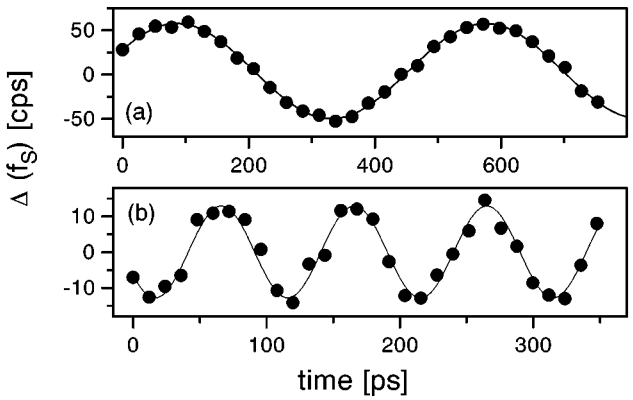


FIG. 13. Microwave signal at the frequencies: (a) $f_s = 2.043$ GHz and (b) $f_s = 10.065$ GHz ($f_i = 5$ kHz, $U_{\mathrm{dc}} = +4$ V).

## V. CONCLUSIONS

In conclusion, we have performed a comprehensive analysis of the effects of static and high-frequency electric fields in silicon MS and MOS structures on optical SHG. Both, linear and paraboliclike bias dependences of the EFISHG response have been found. In the former case the width of the silicon SCR exceeds the volume generating the SH signal, and hence only a small part of the voltage drop in the SCR contributes to the EFISHG response, whereas in the latter case the silicon SCR is screened by photogenerated free carriers or the SH penetration depth exceeds the width of the SCR. The results are in good agreement with theoretical predictions based on a general Green's function formalism,[21] which directly takes into account the spatial distribution of the bias field in the silicon SCR. Furthermore, measurements of the azimuthal SH anisotropy from Si(111) MOS and Si(001) MS interfaces have been performed in the presence of a reverse bias allowing a clear separation of various anisotropic contributions resulting from inhomogeneous bias fields and anisotropic $\chi^{(2)}$ or $\chi^{(3)}$ tensor elements. Finally, we have demonstrated the capability of EFISHG for time-resolved measurements of free-running GHz signals on silicon millimeter-wave devices using a femtosecond Ti:sapphire laser. Such a system greatly simplifies high-frequency testing of silicon integrated devices with sampling bandwidths up to 100 GHz. The sensitivity of the EFISHG method in its present form should permit real-time mapping of subvolt signals in Si MMIC's. Further studies are being performed in this laboratory at photon energies of the fundamental below the indirect Si band gap in order to reduce the invasiveness of the EFISHG technique caused by photogenerated carriers.

[1] J.-F. Luy and P. Russer, *Silicon-Based Millimeter-Wave Devices*, Springer Series in Electronics and Photonics Vol. 32 (Springer, Berlin, 1994).

[2] K. E. Meyer and G. A. Mourou, in *Picosecond Electronics and Optoelectronics*, edited by G. Mourou, D. M. Bloom, and C. Lee, Series on Electrophysics, Vol. 21 (Springer, New York, 1985) pp. 46–49.

[3] W. Mertin, C. Roths, F. Taenzler, and E. Kubalek (unpublished).

[4] B. H. Kolner and D. M. Bloom, IEEE J. Quantum Electron. **QE-22**, 79 (1986).

[5] K. J. Weingarten, M. J. W. Rodwell, and D. M. Bloom, IEEE J. Quantum Electron. **QE-24**, 198 (1988).

[6] H. P. Feuerbaum, Scanning **5**, 14 (1983).

[7] F. J. Henley, in *IEEE MTT-S International Microwave Sympo-*

*sium Digest*, edited by W. R. Scott (IEEE, Piscataway, NJ, 1993), p. 1351.
[8] H. K. Heinrich, D. M. Bloom, and B. R. Hemenway, Appl. Phys. Lett. **48**, 1066 (1986).
[9] O. A. Aktsipetrov, A. A. Fedyanin, V. N. Golovkina, and T. V. Murzina, Opt. Lett. **19**, 1450 (1994).
[10] P. Godefroy, W. de Jong, C. W. van Hasselt, M. A. C. Devillers, and T. Rasing, Appl. Phys. Lett. **68**, 1981 (1996).
[11] J. I. Dadap *et al.*, Phys. Rev. B **53**, R7607 (1996).
[12] G. Lüpke *et al.*, Opt. Lett. **20**, 1997 (1995).
[13] O. A. Aktsipetrov *et al.*, Kvant. Elektron. (Moscow) **19**, 869 (1992) [Sov. J. Quantum Electron. **22**, 807 (1992)].
[14] J. Krueger, N. Sorg, J. Reif, and W. Kautek, Appl. Surf. Sci. **69**, 388 (1993).
[15] J. L. Daschbach, P. R. Fischer, D. E. Gragson, D. Demarest, and G. L. Richmond, J. Phys. Chem. **99**, 3240 (1995); **99**, 10 690(E) (1995).
[16] C. Ohlhoff *et al.*, Appl. Phys. Lett. **68**, 1699 (1996).
[17] A. Nahata, J. A. Misewich, and T. F. Heinz, Appl. Phys. Lett. **69**, 746 (1996).
[18] J. Qi, M. S. Yeganeh, I. Koltover, A. G. Yodh, and W. M. Theis, Phys. Rev. Lett. **71**, 633 (1993).
[19] O. A. Aktsipetrov and E. D. Mishina, Dok. Akad. Nauk SSSR **274**, 62 (1984) [Sov. Phys. Dokl. **29**, 37 (1984)].
[20] O. A. Aktsipetrov *et al.*, Phys. Rev. B **54**, 1825 (1996).
[21] J. E. Sipe, J. Opt. Soc. Am. B **4**, 481 (1987).
[22] U. Emmerichs *et al.*, J. Vac. Sci. Technol. B **12**, 2484 (1994).
[23] J. E. Sipe, D. J. Moss, and H. M. van Driel, Phys. Rev. B **35**, 1129 (1987).
[24] J. G. Mihaychuk, J. Bloch, Y. Liu, and H. M. van Driel, Opt. Lett. **20**, 2063 (1995).
[25] J. Bloch, J. G. Mihaychuk, and H. M. van Driel, Phys. Rev. Lett. **77**, 920 (1996).
[26] C. Meyer *et al.*, J. Vac. Sci. Technol. B **14**, 3107 (1996).
[27] K. S. Giboney, T. Scott, M. J. W. Rodwell, and J. E. Bowers, IEEE Photon. Technol. Lett. **6**, 1353 (1994).
[28] T. Löffler, T. Pfeifer, H. G. Roskos, and H. Kurz, IEEE Photon. Technol. Lett. **7**, 1189 (1995).
[29] Y. R. Shen, *The Principles of Nonlinear Optics* (Wiley, New York, 1984).